Dynamics of transient eddy above rolling-grain ripples

Germain Rousseaux[a] and Harunori Yoshikawa[b]
Physique et Mécanique des Milieux Hétérogènes, UMR 7636 CNRS-ESPCI, 10 Rue Vauquelin, 75231 Paris Cedex 05, France

Alexandre Stegner[c]
Laboratoire de Météorologie Dynamique, ENS, 24 Rue Lhomond, 75005 Paris, France

José Eduardo Wesfreid[d]
Physique et Mécanique des Milieux Hétérogènes, UMR 7636 CNRS-ESPCI, 10 Rue Vauquelin, 75231 Paris Cedex 05, France

(Received 30 June 2003; accepted 8 January 2004; published online 8 March 2004)

This study deals with the flow motion over the so-called rolling-grain ripples which are generated by water oscillations above a sand bed. We focus our efforts on quantifying by means of laboratory experiments and numerical calculations the morphology and the dynamics of transient flow patterns. We report, for the first time, on the formation of an unsteady pattern with closed streamlines (we call it ''eddy'') above rolling-grain ripples using flow visualizations and particle image velocimetry measurements. This structure appears in the ripple trough during flow reversal and scales with the ripple wavelength. The experimental results are in qualitative agreement with the perturbative flow solution calculated by Vittori in 1989. Even if the relative ripple amplitude is not small in the experiment the perturbative expansion at the first order gives an accurate description of the flow dynamics. © *2004 American Institute of Physics.* [DOI: 10.1063/1.1651482]

I. INTRODUCTION

Ripples are very fascinating patterns which occur on sandy beaches and are created by the back and forth motion induced by gravity waves in the water. Since the seminal work of Bagnold,[1] two types of patterns have been distinguished: rolling-grain ripples and vortex ripples. Bagnold introduced this terminology to describe small patterns with grains moving to and fro at the interface between sand and water (the rolling-grain ripples) and larger patterns with a vortex detaching from the crest scooping grains from the neighboring sand structures (the vortex ripples). Since then, the appearance of transient vortices above a ripple bed is generally assumed to be the dynamical signature of the vortex ripple pattern. This typical pattern corresponds to a large amplitude perturbation of the initially flat sand bed with a maximum slope close to the avalanche angle of the granular medium.[2] The large angle of the pattern is assumed to be responsible for the flow separation behind the crest which induces the vortex formation.[3] On the other hand, rolling-grain ripples correspond to weak perturbations of the sandy bottom having small slopes. In this limit, asymptotic expansion could be used to estimate theoretically the first-order correction to the flow field induced by an infinitely small wavy wall below an oscillating Stokes layer.

In the two dimensional (2D) infinite-depth case, one can describe the problem with only three dimensionless parameters: ϵ, Re_δ, and r where ϵ is half the ripple height h scaled by the Stokes layer thickness $\delta=\sqrt{\nu/\pi f}$, Re_δ the Reynolds number defined with δ, and r the ratio of the fluid displacement $2A$ to the bottom wavelength λ: $\epsilon=h/2\delta$, $\mathrm{Re}_\delta=2A/\delta$, and $r=2A/\lambda$, where ν is the kinematic viscosity and f the oscillation frequency. We illustrate in Fig. 1 the range of the parameters ϵ and r corresponding to both previous and present works.

The coupling between the frequency of the main Stokes flow and the intrinsic frequency induced by the wavy bottom perturbation generates a steady-flow component. Such a phenomenon is often encountered in oscillatory flow and is known as steady streaming.[4–6] Lyne[7] investigated the problem for the case of small height $\epsilon \ll 1$ and $r \gg 1$ or $r \ll 1$ and he showed that a solid wavy wall could create steady recirculations directed from the troughs to the crests. Sleath[8] pointed out that rolling-grain ripples can be produced by such steady secondary flows. Kaneko and Honji[9] considered higher-order solutions in the parameter ϵ under the condition that the fluid displacement is very small ($r \ll 1$). Recently, Cuevas *et al.*[10] obtained analytical results using a double expansion in the parameter r and ϵ ($r \ll 1$ and $\epsilon \ll 1$). They performed this study when a vertical magnetic field acting on an electrical conducting liquid damps the steady streamings. However, as noticed by Sleath,[8] natural ripples form for values of r of order one. Therefore, Blondeaux and Vittori[11–13] extended the theoretical analysis for arbitrary value of r when $\epsilon \ll 1$. Performing a standard linear stability analysis, Blondeaux explained the formation of rolling-grain ripples by the following mechanism:[12] small perturbations of the initial flat bed creates recirculating cells (steady streamings)

[a]Present address: Institut Non-Linéaire de Nice, Sophia-Antipolis, UMR 6618 CNRS, 1361 route des Lucioles, 06560 Valbonne, France; electronic mail: germain.rousseaux@inln.cnrs.fr
[b]Electronic mail: harunori@pmmh.espci.fr
[c]Electronic mail: stegner@lmd.ens.fr
[d]Electronic mail: wesfreid@pmmh.espci.fr

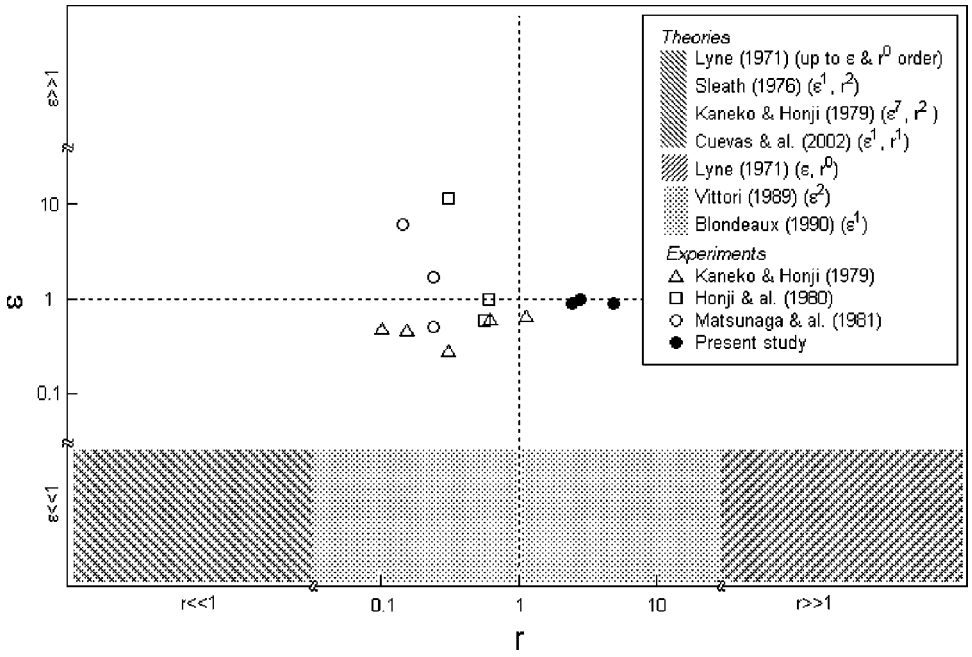

FIG. 1. Phase plane $r-\epsilon$ for the existing theories and experiments on flow over rolling-grain ripples.

which are directed from the through to the crest of the ripple's nucleus and then contribute to the long time average of the growth of the initial perturbation by enhancing the sediment transport directed toward the crest. Each ripple features at least two steady cells on both slopes whose form and intensity depend on the instability parameters.[8–15] Nevertheless, in both nature and laboratory experiments, one can hardly detect rolling-grain ripples having amplitudes below two or three grain diameters[16] and well defined patterns are generally obtained only for finite values of ϵ (Fig. 1). Therefore, the validity of these asymptotic calculations for real sand patterns remains unclear. Besides, the stability of the perturbative solutions, namely the possible flow separation and vortex detachment, are still under question for a finite value of ϵ.

Several recent studies try to reproduce sand ripples in the laboratory. Until now, the main research was focused on the vortex ripples wavelength selection[2,17–19] and hydrodynamics.[1,17,19] Recently, we showed that the rolling-grain ripple state always evolves to a final vortex ripple state and never stabilizes contrary to what was proposed by Bagnold.[2] Similar conclusions were reported by Faraci and Foti.[18] As far as laboratory investigations are concerned, quantitative flow measurements with real rolling-grain ripples are quite difficult due to the high spatial resolution (below 0.1 mm) needed to measure accurately their morphology.[16] The experiments of Kaneko and Honji[9] using a weakly stratified fluid in glycerin–water solutions and shadowgraph techniques allow one to visualize the averaged circulations which affect the mean vertical stratification after several oscillations. These experiments, which correspond to $\epsilon \simeq 0.2-1$, $\mathrm{Re}_\delta \simeq 2-20$, and $r<1$ or $r>1$, exhibit well-defined steady recirculating cells analogous to the calculated steady streaming. With Matsunaga, they confirmed the presence of steady cells for the cases $\epsilon \gtrsim 1$ in stratified glycerin–water solutions with glass beads when $r<1$.[14,20] They also reported steady cells in water for $r<1$ above ripple models corresponding to dye streaklines[20] or aluminum dust[14] visualization for $\epsilon>1$. However, to measure the instantaneous flow field above rolling-grain ripples, short-time consecutive images at high spatial resolution are needed.

In the present study we measure for the first time the instantaneous flow field above rolling-grain ripples using a high speed video camera to perform particle image velocimetry (PIV). We focus our investigation on the formation of transient-vortex structures which differ significantly from the steady streamings and appear in the following range of parameters: $r>1$, $\mathrm{Re}_\delta \simeq 40-50$, and $\epsilon \gtrsim 1$.

In Sec. II, we describe the experimental setup and techniques. In Sec. III, we use the first-order expansion of Vittori[11] to calculate numerically the periodic flow above monochromatic ripple patterns: combination of the main Stokes flow and the first-order correction (which includes steady and unsteady motion). The comparison of this theoretical estimation, valid for $r \simeq 1$ and $\epsilon \ll 1$ with the experimental results analysis, is done in Sec. IV.

II. EXPERIMENTAL SETUP AND TECHNIQUES

Underwater sand ripples can be reproduced in the laboratory when a layer of sand is put on a smooth plate which oscillates horizontally in static water. The velocity of the plate diffuses into the fluid by viscosity over a typical scale which is two or three times the Stokes-layer thickness. For sizes smaller than the Stokes layer, the grains are submitted to uniform and oscillating shear stresses analogous to the back and forth motion induced by water waves on the sand bed at the beach.[21]

The principle of the setup is described in Stegner and Wesfreid[2] but a new facility was built in order to perform flow visualizations. It consists of two concentric cylinders of Plexiglass which are linked on the top and the bottom by two

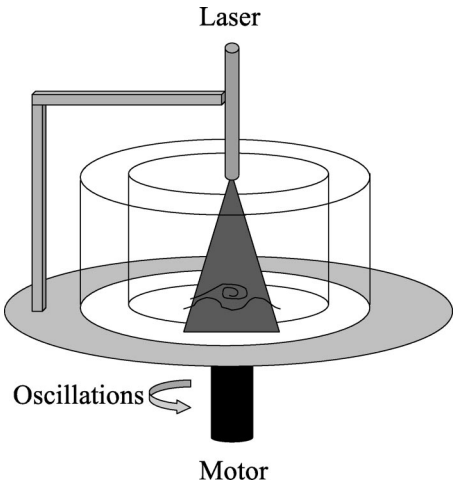

FIG. 2. Experimental setup.

circular plates (Fig. 2). The bottom plate is driven by a brushless motor which oscillates at a fixed displacement amplitude A and frequency f. The top plate is made of transparent Plexiglass. The mean radius of the cylinders is 135.5 mm and the gap size between the cylinders is 19.0 mm. We put a layer of monodisperse spherical glass beads (diameter $d=0.11$ mm$<\delta=0.56$ mm at 1 Hz and density $\rho_s=2.49\times10^3$ kg/m^3) between the cylinders and fill the gap with water. We use the circular geometry in order to have spatially periodic boundary conditions. When the oscillations are occurring, the water shears the bed and the grains move to and fro at the interface:[1] rolling-grain ripples are created all along the perimeter and then start to grow by coalescence. When the height reaches a critical value, vortex ripples appear and grow by both coalescence and annihilation until they reach a final state with a wavelength which is 4/3 of the amplitude of oscillation in a first approximation.[2]

In order to visualize the flow patterns, the water is seeded with a plastic powder ORGASOL (diameter $d_p=0.06$ mm and density $\rho_p=1.03\times10^3$ kg/m^3) that reflects light. We generate a laser sheet in the middle of the gap with a laser diode from Lasiris (685 nm, 50 mW) which is embarked on the setup (Fig. 2) as a charge coupled device (CCD) camera with a macro zoom (12.5–75 mm). Flow visualizations are done with a CDD camera at 25 images/s. In addition, we perform PIV with a high-speed video camera (FastCam Super 10 k from Photron: 250 pictures/s and 540 $\times480$ resolution) under continuous light from the laser diode. The resolution is 0.047 mm per pixel in our experiments. The image processing is done on a personal computer with the software Davis 6.2 and PIV with algorithms from Lavision. We used the so-called ''multipass'' calculations starting from a 64×64 pixels by pixels interrogation window to a 12×12 pixels by pixels window in order to compute the velocity vectors.

III. NUMERICAL CALCULATIONS

In this section we recall the first-order expansion of the transient flow generated by water oscillations over a rigid wavy wall. Several methods for the calculation can be found in the literature[7–12,14,15,22] when the geometrical length scale λ is larger than the bottom boundary layer δ. Although all of them can predict not only time averaged but also transient flow, the characteristic features of the latter have not been documented so far except by Hara and Mei for the vorticity patterns.[22] Among those methods, we adopt the one introduced by Vittori[11] which determines 2D flow over a small wavy wall and keeps applicability up to large values of the dimensionless parameter $r=2A/\lambda$ as in our experiments ($r=2.73$: experiment 3 in Table I). The streamfunction ψ of the flow over a sinusoidal wavy bottom generated by an ambient flow oscillation is described by the following dimensionless equation and boundary conditions:

$$2\frac{\partial\Delta\psi}{\partial t}+\mathrm{Re}_\delta\left[\frac{\partial\psi}{\partial y}\frac{\partial\Delta\psi}{\partial x}-\frac{\partial\psi}{\partial x}\frac{\partial\Delta\psi}{\partial y}\right]=\Delta^2\psi, \tag{1}$$

$$\frac{\partial\psi}{\partial y}=0,\quad -\frac{\partial\psi}{\partial x}=0,\quad \text{at}\quad y=\epsilon\cos(\alpha x), \tag{2}$$

$$\frac{\partial\psi}{\partial y}\to\cos t,\quad -\frac{\partial\psi}{\partial x}\to0,\quad \text{when}\quad y\to\infty, \tag{3}$$

where all lengths are scaled by the Stokes layer δ and Re_δ is defined by: $\mathrm{Re}_\delta=2\pi fA\delta/\nu=2A/\delta$. The horizontal and vertical coordinates are x and y. The bottom surface is represented by $y=\epsilon\cos(\alpha x)$, where α is the dimensionless wave number of the bottom waviness scaled by δ^{-1}. The periodic solution of this problem is given in the following form:

$$\psi=y\cos t+\frac{1}{\sqrt{2}}e^{-y}\cos(t-y-\pi/4)+\frac{\epsilon}{2}\left[\sum_{m=-\infty}^{\infty}G_m(y)e^{\mathrm{i}mt}e^{i(\alpha x-\pi r\sin t)}+\text{c.c.}\right]+O(\epsilon^2), \tag{4}$$

where the first and second terms of the right-hand side constitute the $O(1)$-order solution of the problem. Vittori expressed the second term in the complex representation and

TABLE I. Experimental parameter values. The laminar Shield number Θ_L is defined as $\Theta_L=2\pi fA\rho_f\nu/\Delta\rho g\delta d$.

Parameters	f (Hz)	δ (mm)	A (mm)	Θ_L	λ (mm)	h (mm)	ϵ	Re_δ	r
Experiment 1	1	0.56	12	0.08	~10	1	0.88	42.6	~2.4
Experiment 2	1	0.56	15	0.1	22	4	3.55	53.2	1.36
Experiment 3	1	0.56	15	0.1	11	1.1	0.98	53.2	2.73

did not write the first term because she worked in the reference frame oscillating with the ambient flow while our (numerical or experimental) frame is at rest with respect to the wavy bottom. The third term is the $O(\epsilon)$ solution; the factor $e^{i(\alpha x-\pi r\sin t)}$ enables us to transform the Vittori's $O(\epsilon)$-order solution into the one for our reference frame. $G_m(y)$s are complex functions to be determined by the following set of ordinary differential equations and their boundary conditions:

$$(D^2-\alpha^2)(D^2-\alpha^2-i2m)G_m(y) = -i\pi r[e^{-(1+i)y}(D^2-\alpha^2-i2)G_{m-1} + e^{-(1-i)y}(D^2-\alpha^2+i2)G_{m+1}], \quad (5)$$

$$(DG_m)_{y=0}=-\frac{1+i}{2}J_{m-1}(\pi r) - \frac{1-i}{2}J_{m+1}(\pi r), \quad (G_m)_{y=0}=0, \quad (6)$$

$$(DG_m)_{y\to\infty}=0, \quad (G_m)_{y\to\infty}=0, \quad (7)$$

where D denotes differentiation with respect to the y. $J_m(\xi)$ is the first kind Bessel function of order m

$$J_m(\xi)=\frac{1}{2\pi}\int_{-\pi}^{\pi}e^{i\xi\sin t'}e^{-im t'}dt'. \quad (8)$$

Because of the boundary conditions at infinity, the right-hand side of (5) becomes so small sufficiently away from the bottom boundary layer that the solutions there are given in terms of two sets of unknown constants a_m and b_m

$$G_m(y_0)=a_m e^{-\alpha y_0}+b_m(1-\delta_{m0}+\delta_{m0}y_0)e^{-\sqrt{\alpha^2+i2m}y_0}, \quad (9)$$

where δ_{m0} is the Kronecker delta.

Then, the set of ordinary differential equations (5) can be integrated numerically as an initial-value problem from a sufficiently large $y=y_0$ out of the bottom boundary layer. The unknown constants a_m and b_m appear throughout the integration and are finally determined by the boundary conditions at the bottom (6) for the calculated values of $DG_m(y=0)$ and $G_m(y=0)$, which are linear combinations of a_ms and b_ms. Actually, for given t, α, and Re_δ, the infinite series in (4) is truncated at a sufficiently large integer $m=\pm M$ and the following symmetry conditions are used to reduce the number of unknown constants:

$$a_{-m}=(-1)^{m+1}a_m^*, \quad b_{-m}=(-1)^{m+1}b_m^*, \quad (10)$$

where $*$ denotes the complex conjugate. The $2(M+1)$ unknown constants of a_m and b_m $(m=0,1,...,M)$ are then determined by the $2(M+1)$ boundary conditions (6) for G_m and DG_m $(m=0,1,...,M)$. Once we know the value of the constants a_m and b_m, we can calculate the G_ms with which (4) gives the instantaneous streamfunction. By varying the time t, we obtain a series of streamlines and we can infer theoretical predictions for the flow evolution. For the averaged flow, we insert the determined G_ms into the following equation, which has been obtained by averaging Eq. (4) with respect to time:

$$\overline{\psi}=\frac{\epsilon}{2}\left[\sum_{m=-\infty}^{\infty}J_m(\pi r)G_m(y)e^{i\alpha x}+\text{c.c.}\right]+O(\epsilon^2). \quad (11)$$

We can thus obtain both averaged [Fig. 3(left)] and instantaneous [Fig. 3(right)] flow patterns. As will be seen later, our calculations predict short life eddies and these are compared with the experimental results below.

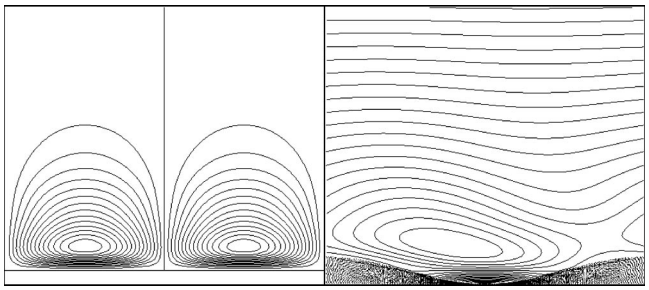

FIG. 3. Comparison between the averaged flow (left) and an instantaneous vortical structure (right) over the rolling-grain ripples ($\Delta\phi=0.01$ for the former and $\Delta\phi=0.1$ for the latter). The parameters are $\alpha=0.322$, $\mathrm{Re}_\delta=53.2$, and $\epsilon=0.98$, which correspond to experiment 3 in Table I. The time $t/T=-0.1$ has been chosen for the instantaneous flow pattern.

IV. RESULTS AND DISCUSSION

A. Experimental results

The parameters for the experiments are reported in Table I where we compute some nondimensional parameters used in the context of bedforms like the laminar Shields number Θ_L which is the ratio of the laminar shear force on one grain $\tau_L d^2\simeq\rho_f\nu(V/\delta)d^2$ to its reduced weight $\Delta\rho g d^3$, where $V\simeq 2\pi fA$ is the background flow velocity and $\Delta\rho$ the difference between solid and fluid density.

After few oscillations of the experimental apparatus, the initially flat sand–water interface exhibits a ripple pattern. At the beginning of the instability, it is hard to distinguish coherent structures in the flow above sand patterns. Indeed, the height of the first patterns is about 2 or 3 grain diameters. Afterwards, the ripples experience some coalescence events. The ripples amplitudes keep on growing and then we can observe transient eddies in the flow. Better visualizations of the flow pattern are, of course, realized for higher rolling-grain ripples as those just before the transition to the vortex ripple regime for height on the order of 1 mm. We show an example of the flow pattern above rolling-grain ripples during a coalescence in Fig. 4. Here, we can see only one eddy or pattern with closed streamlines in each ripple trough. Note

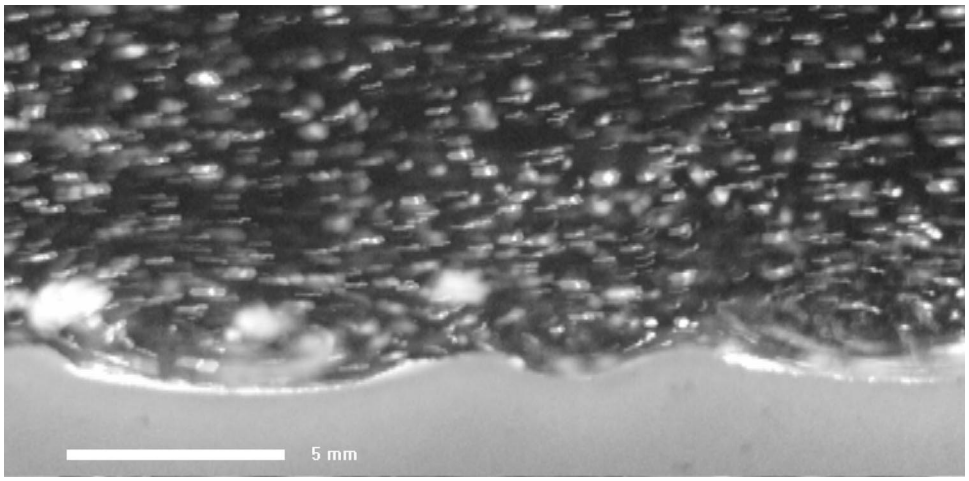

FIG. 4. Visualization of the flow pattern over rolling-grain ripples during a coalescence for $A=12$ mm, $f=1$ Hz, and $d=0.11$ mm.

that the horizontal extension of the eddies over rolling-grain ripples is fixed by the distance between two ripple crests. The experimental flow parameters here are $\epsilon=0.88$, $\mathrm{Re}_\delta=42.5$, and $r=2.4$ corresponding to experiment 1 (see Table I). Later in time rolling-grain ripples experience a transition to the vortex ripple regime. During this transition, the ripples grow rapidly, accompanying the appearance of large vortices.[2] The ripples finally reach a relatively fixed state which slightly evolves on very long times. We can observe a vortex detaching from each ripple crest twice during one oscillation period. Unlike the transient eddies described in Fig. 4, the horizontal vortex size over vortex ripples is roughly equal to half a ripple wavelength (Fig. 5 for $\epsilon=3.55$, $\mathrm{Re}_\delta=53.2$, and $r=1.36$, corresponding to experiment 2 of Table I).

An important characteristic of the eddies observed above rolling-grain ripples is that they are short lived. These transient structures appear while the flow reverses its direction of motion. Unlike the vortex-ripples vortices as the one shown in Fig. 5, these eddies remain coherent for only a very short time compared to half of the ambient-flow oscillation period $T/2$. From the PIV, we compute the velocity vectors of these transient structures over rolling-grain ripples (Fig. 6) and we can display the associated streamlines.

Indeed, instantaneous streamlines showing the dynamical evolution of these eddies are presented in Fig. 7. Here $\epsilon=0.98$, $\mathrm{Re}_\delta=53.2$, and $r=2.73$ corresponding to experiment 3 in Table I (note the difference of scalings between experimental and theoretical images in Figs. 7 and 8 as mentioned in the legends). In this case, the observed eddy remains coherent for roughly 70 ms, that is to say, around one seventh of $T/2$ ($T=1$ s). In contrast with the steady cells shown in Kaneko and Honji[9] by glycerin–water stratification, the observed transient cells exist one per trough, corotating together. Each of them occupies all length over a trough and has a vertical size around twice the ripple height [Fig. 7(b)]. It grows vertically and then is ejected from the bottom. After the ejection, the elliptical eddy deforms its shape as shown in Fig. 8(a). We note here that the vertical position of the eddy's center seems to follow the flow reversal line of the unperturbed Stokes layer. After the ambient flow reversal, this structure disappears in a very short time. Then, a simple unidirectional shearing can be seen. The observation of the eddy's birth is difficult due to its size, which is on the order of the Stokes layer. Besides, the settled plastic particles and disturbed sand grains introduce a large scale noise on the video image which affects the PIV resolution. Sometimes we notice that the eddy appears on the lee side of

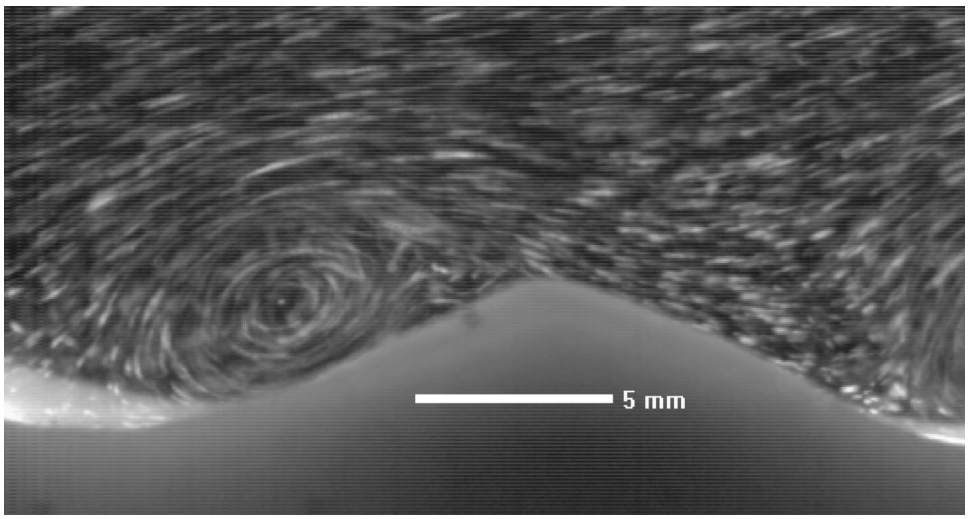

FIG. 5. Visualization of the flow pattern over a vortex ripple for $A=15$ mm, $f=1$ Hz, $d=0.11$ mm: we superimposed four successive images taken at 250 pictures/ps. The background flow goes to the left.

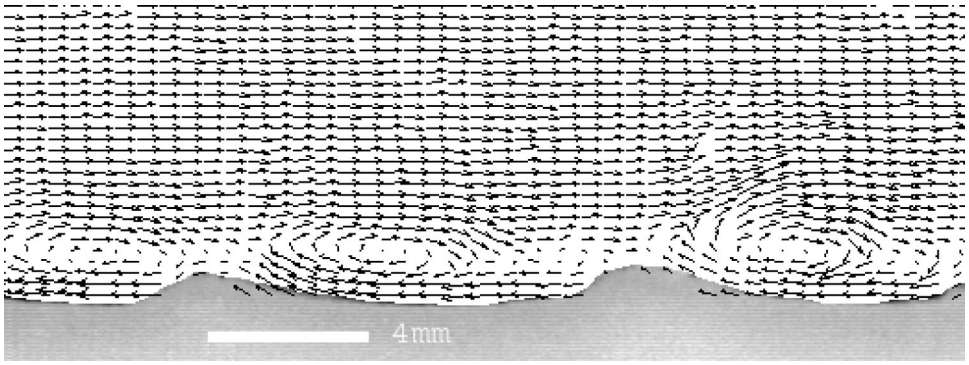

FIG. 6. Velocity vectors of the transient eddies above rolling grains ripples for $A=15$ mm, $f=1$ Hz, $d=0.11$ mm, $t^*f=1620$ (number of oscillations), and 32 ms before flow reversal. The background flow goes to the right.

ripples and grows horizontally to occupy the whole space between two neighboring ripple crests.

Quantitative measurements of the velocity and the vorticity of the transient eddy corresponding to Fig. 7(b) are obtained from the PIV. For this case, the maximum velocity ($V\simeq 23$ mm/s) and vorticity ($\omega\simeq 28$ rad/s) of the eddy remains smaller than the maximum velocity ($V=95$ mm/s) and vorticity ($\omega=167$ rad/s) of the main oscillating Stokes flow. Hence, even if the relative ripple height $\epsilon=0.98$ is close to unity, the amplitude of the perturbed flow (i.e., velocity and vorticity of the transient vortex) would be less than one third of the maximum unperturbed Stokes flow.

B. Numerical results and comparisons

Numerical calculations with different parameter values in the regime $r>1$ predict the appearance of one eddy or structure with closed streamlines above each ripple trough twice during an ambient flow oscillation. We show, on the right half of Figs. 7 and 8, the calculated streamlines having the same parameters ($\epsilon=0.98$, $\mathrm{Re}_\delta=53.2$, and $r=2.73$) as

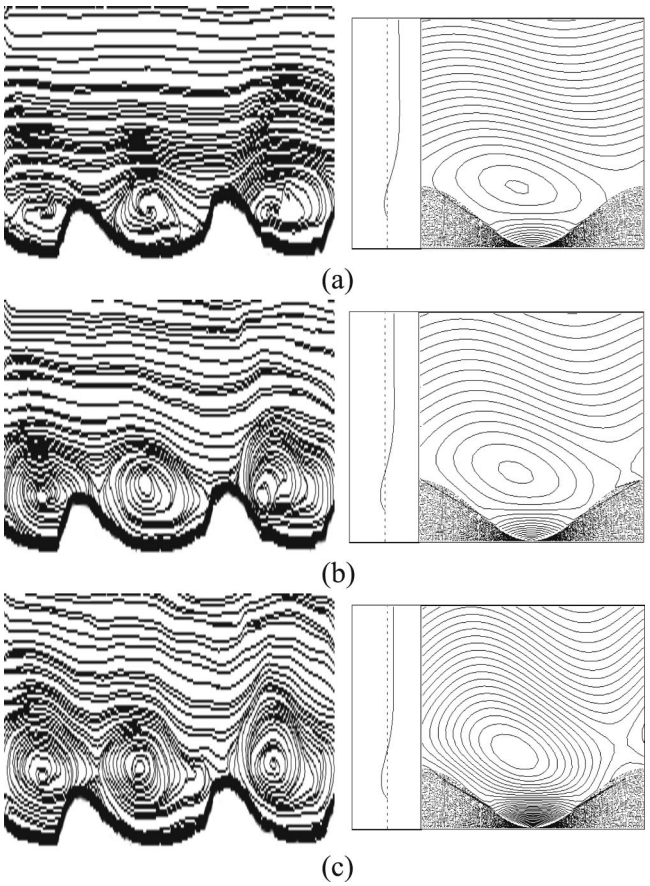

FIG. 7. Development of the eddy over the rolling-grain ripples for $A=15$ mm, $f=1$ Hz, $d=0.11$ mm, and $t^*f=1620$ (number of oscillations). Experimental and numerical streamlines with the Stokes background flow profile ($\Delta t=16$ ms). (a) is 60 ms before flow reversal. For the experimental (numerical) images, the height is 4.1 mm and the width is 24.5 mm (11 mm). The background flow goes to the right.

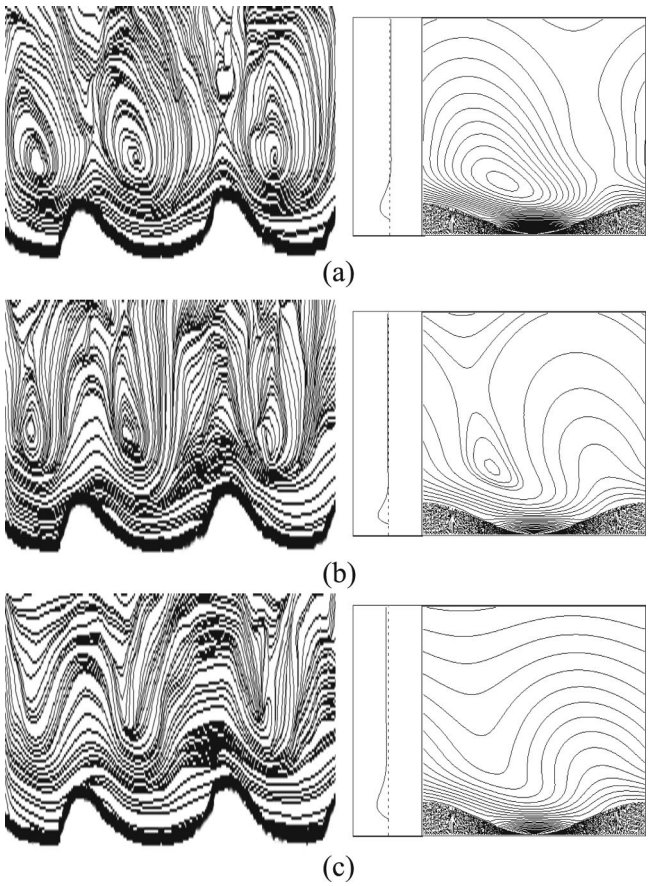

FIG. 8. Ejection and death of the eddy over the rolling-grain ripples for $A=15$ mm, $f=1$ Hz, $d=0.11$ mm, and $t^*f=1620$ (number of oscillations). Experimental and numerical streamlines with the Stokes background flow profile ($\Delta t=8$ ms). (d) is 4 ms before flow reversal. For the experimental (numerical) images, the height is 4.1 mm (7.7 mm) and the width is 24.5 mm (11 mm).

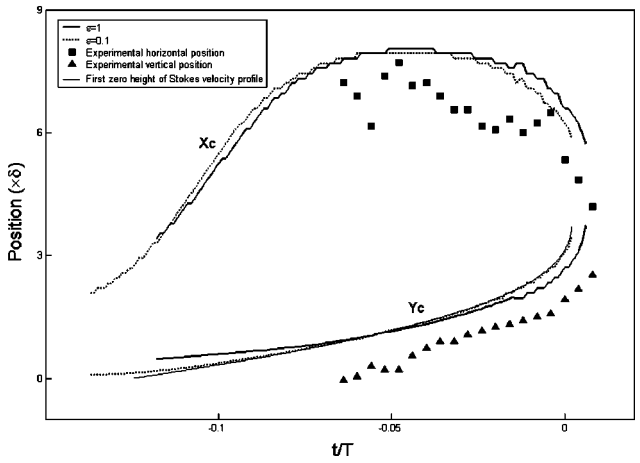

FIG. 9. Position of the eddy's center for $A=15$ mm, $f=1$ Hz, $d=0.11$ mm, and $t^*f=1620$ (number of oscillations). $t=0$ corresponds to flow reversal.

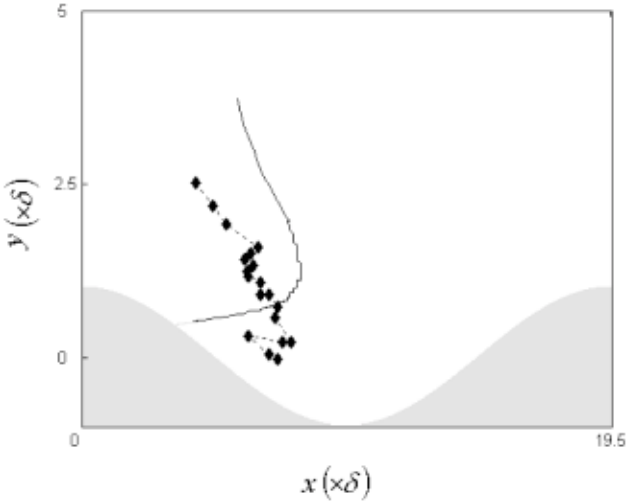

FIG. 10. Trajectory of the eddy's center for $A=15$ mm, $f=1$ Hz, $d=0.11$ mm, and $t^*f=1620$ (number of oscillations).

the experiment. We have truncated the series (4) at $M=25$ to calculate the numerical streamlines and compared them with the experimental ones at the same instant. The velocity profiles of the unperturbed Stokes flow above a flat bottom are also shown in the middle of Figs. 7 and 8.

Surprisingly, even if the validity of the asymptotic expansion (detailed in Sec. III) is seemingly in question for $\epsilon=1$, the first-order calculation seems to capture correctly the dynamics of the transient eddy observed in the experiment. In Fig. 7(a), we can see an eddy turning clockwise above the trough. It occupies the whole length over the ripple trough and its center is located above the midthrough slightly upstream. The calculated transient vorticity ($\omega \simeq 30\ \mathrm{rad\,s^{-1}}$) is in very good agreement with the vorticity estimated in the experiment ($\omega \simeq 28\ \mathrm{rad\,s^{-1}}$). This eddy stays in the middle of the trough while it grows along the vertical. Then, it is deformed towards the upstream left crest [Figs. 7(b) and 7(c)]. After this growth process, the eddy is ejected and significantly deformed, enlarging vertically again. The center shifts upstream as it rises [Fig. 8(a)]. This ejected eddy significantly deforms to a quasitriangular shape just after the ambient flow reversal [Fig. 8(b)]. Then, the eddy disappears within a very short time. It rapidly shrinks and disappears [Fig. 8(c)] within a layer of thickness approximately equal to $\lambda/3$.

In order to quantify more precisely the dynamics of this transient structure, we have plotted its vertical and horizontal positions (Fig. 9) as well as its path over the ripple through (Fig. 10). The zero for the horizontal (vertical) position corresponds to the left crest (the mid height of the ripple). As far as the eddy's position is concerned, there is a correct agreement between the numerical calculation and the laboratory observations, even if the theoretical predictions slightly overestimate the vertical and the horizontal positions. Besides, the first-order expansion gives important results about this position at the very beginning of the eddy's appearance which cannot be detected in the experiments. In particular, one can observe a clear increase of the horizontal position at the beginning before reaching a plateau close to the center of the ripple trough. Afterwards, the eddy's center is shifted upstream before its death (Fig. 10). It is important to note that the calculated positions do not depend on the value of ϵ (Fig. 9). Hence, the eddy's path will be the same for both small and finite ripple amplitudes. In fact, the vertical position of the eddy follows the null-velocity position of the unperturbed Stokes flow.

Nevertheless some discrepancies appear between the calculated and observed streamlines. The asymptotic expansion predicts a strong reverse shear below the transient eddy which is not observed in the experiment. Besides, these streamlines intersect the ripple interface, which correspond to a nonphysical transverse velocity. Hence, the validity of the first order expansion is broken for the boundary condition when ϵ reaches a finite value. Unlike the analytical model, the experimental shape of the ripple is not sinusoidal. This could also introduce some discrepancies between the calculated and observed streamlines. Moreover, we assumed a no-slip boundary condition in the calculations, whereas a small slip velocity at the interface between a fluid and a porous media could occur.[23,24]

Unlike laboratory measurements which have limited resolution, the numerical calculations give information on the initial generation of the transient eddy along the bottom Stokes boundary layer. The eddy generates at a very small size on the lee side of ripple crests and enlarges horizontally to occupy all the wavelength over the ripple trough. This process could not be observed clearly in our experiments because of the size of the Stokes layer, which is about $\delta=0.56$ mm in water at 1 Hz. For the observation on scale comparable to the wavelength λ, the appearance over the trough is very well predicted. Figure 11 shows this process for the parameters of experiment 3 in Table I except for the value of ϵ which is 0.1.

The calculations for $r \ll 1$ also show transient structures during the ambient flow reversal. Parameter dependence of the transient flow structure with r is shown in Fig. 12 at $19T/250$ before the ambient flow reversal for $\alpha=0.322$ and $\epsilon=0.1$. The predicted morphology is very different. Two ed-

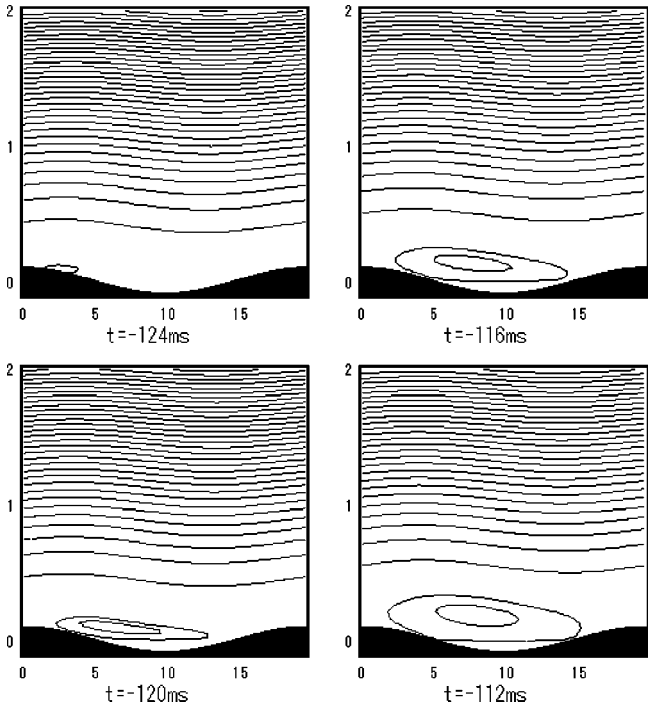

FIG. 11. Birth of the eddy over the rolling-grain ripples for the following parameters: $\alpha=0.322$, $r=2.73$, and $\epsilon=0.1$. The time $t=0$ corresponds to flow reversal. The background flow goes to the right.

dies are generated at the crest and trough, respectively, and both are ejected vertically [Fig. 12(a)]. They merge into one larger eddy above the crest and disappear over the crest. Between the former ($r>1$) and latter ($r\ll 1$) parameter regimes, we have an intermediate one [Fig. 12(b)], where we observe the fusion of two eddies above the ripple lee side. Whether one or two eddies appear would depend on r (notice that we always keep the condition $\lambda>\delta$). In our numerical explorations of the total flow, we always see one vortical structure when $r>1$ and when r is smaller than 1, we observed the merging of two eddies into a larger one. This criterion enables us to distinguish the two regimes and has some relation with Vittori's criterion on the number of steady recirculating cells.[11] Indeed, the curve $r=1$ is similar to the limiting curve of the (α, Re_δ) plane in Fig. 8 of Ref. 11 for the case of $\mathrm{Re}_\delta>10$, which corresponds to real ripples in water (we recall that $\alpha R_\delta=2\pi r$).

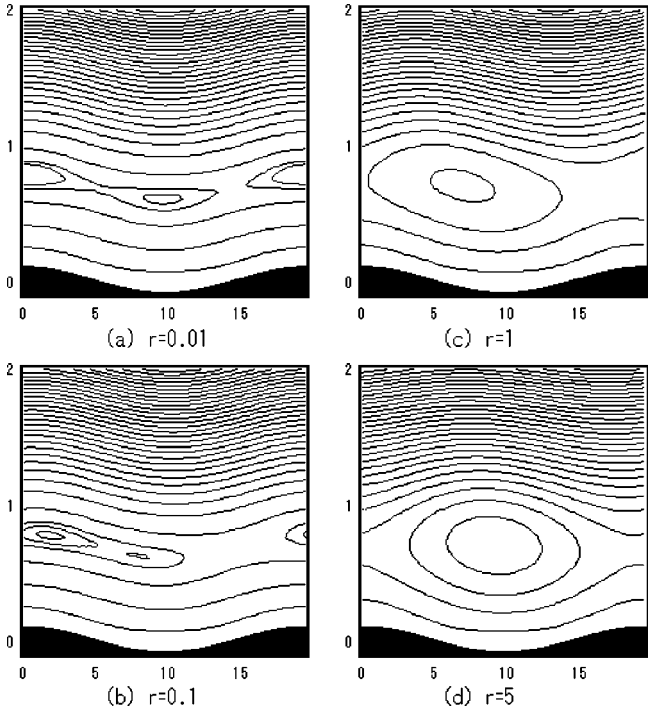

FIG. 12. Dependence of the flow morphology on the r parameter with $\alpha=0.322$ and $\epsilon=0.1$ at $19T/250$ before the ambient flow reversal from the right to the left. The background flow goes to the right.

C. Discussion

Several questions arise from this combined theoretical and experimental investigation. First of all, how far can we rely on the asymptotic calculations of the perturbed flow? Why do these calculations capture correctly the transient vortex dynamic in the range of $\epsilon\simeq 1$ where the validity of the expansion is in principle broken?

In fact, one should keep in mind that the dimensionless wave number α is also a small parameter and that the perturbed flow is controlled both by the ripple height ϵ and the ripple wavelength α. Indeed, if α tends to zero (ripple wavelength tends to infinity) the perturbed flow should vanish, even if we keep $\epsilon\simeq 1$. Hence, we can suspect that the amplitude of the transient eddy scales with the ripple slope $\alpha\epsilon$ rather than relative ripple height ϵ. First-order expansions[11] could be extended up to a large value of ϵ if the ripple slope remains small enough. Moreover, we should note that the correct agreement between the laboratory observation and the theoretical solution shows that this asymptotic solution is robust in the range of parameters studied with respect to the flow structure prediction despite some errors near the bottom boundary layer. Therefore, our results tend to validate the use of laminar asymptotic theory to estimate the perturbed flow above rolling-grain ripples.

To have an idea of the physical origin of this structure, the solutions of the unsteady Stokes equation ($\partial_t\Delta\psi=\nu\Delta^2\psi$) have also been examined. By the same method as described in Sec. III, an explicit expression for the streamfunction is obtained and this streamfunction gives very similar streamlines to those calculated by resolving the full Navier–Stokes equation. By the solution of the unsteady Stokes equation, the appearance of an eddy at flow reversal is predicted and the size and form of the eddy are well described by this solution with a small difference with respect to the horizontal position of the eddy's center. Hence, the eddies observed experimentally are caused by the viscosity and one can infer that fluid inertia does not play the main role during flow reversal that is at the weakest moment of the flow. It is interesting to note that these two kinds of flows are analogous to those observed in the steady flow behind a backwards-facing step or a sudden expansion, where a purely viscous eddy as studied by Moffatt or a vortex formed with the flow separation at the corner of the step is observed, depending on the value of the parameters.[25,26]

The observed vortical structure above rolling-grain

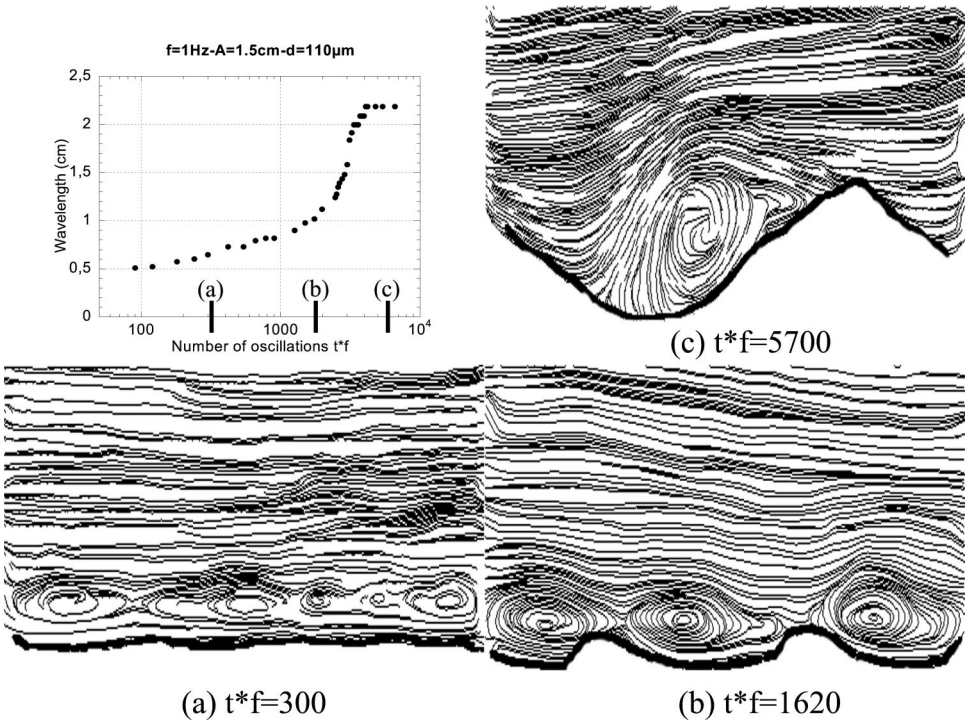

FIG. 13. Evolution of the ripple wavelength in function of the number of oscillations with the corresponding sand morphology and hydrodynamic streamlines for $A=15$ mm, $f=1$ Hz, and $d=0.11$ mm. The transition from rolling-grain ripples to vortex ripples happens around 2000 oscillations.

ripples has a different physical origin from the one above vortex ripples. The former is created by purely viscous effects and does not feature any boundary layer separation, while the latter needs a nonlinear inertial term in the Navier–Stokes equation and always produces the separation. The eddy calculated from the unsteady Stokes equation does not contribute to the averaged flow because of the linearity of the equation.

The transient vortical structure we have observed differs strongly in morphology and amplitude with the flow averaged over one oscillation (steady streaming) (Fig. 3). The comparison between these two structures should be made both on their amplitude and their lifetime. In the case we studied, the vorticity of the transient eddy is higher ($\omega = 30$ rad/s) than the mean vorticity of the averaged flow (10 rad/s), but its lifetime corresponds to roughly $0.15(T/2)$. So the advective effect by this transient structure is roughly 45% of that induced by the averaged flow during $T/2$. Hence, the advective effect of the transient eddy on half a period of oscillation is smaller than but of the same order of magnitude as the averaged flow. Therefore, as far as the transport of passive scalar in the fluid is concerned, the unsteady flow motion should be taken into account. In other words, the streaklines will differ strongly from the averaged streamlines for such unsteady flow. Therefore, attempts at observing the steady streaming cells using dye visualization[14,20] should be taken with care. Besides, if some granular suspension occurs in the flow, the unsteady eddies will have an impact on the global sediment transport. Note that the steady streaming observations of Kaneko and Honji[9] using a weakly stratified fluid were made in a different range of parameters ($r<1$) where, according to Fig. 3, the transient eddy is much smaller in size and has a smaller lifetime. Therefore, we suspect that, in this case, the advections induced by the steady and unsteady flow over one oscillation period are both small. Therefore, the cumulative effect of the steady streaming cells will appear in the stratification after several oscillations.

So far, our experiments focused on the flow over rolling-grain ripples and we therefore presented only one visualization of the flow over a vortex ripple (Fig. 5). That is why we report for completeness the entire evolution of a water–sand interface and of the corresponding streamline patterns [Figs. 13(a), 13(b), and 13(c)]. In this last figure, we can see a well developed vortex above the lee side of a triangular-like vortex ripple in addition to the flow separation close to the crest. Slightly downstream of the vortex, we notice that the streamlines which escape from the vortex follow the ripple profile. This flow structure is similar to the steady flow over a backward-facing step.

Finally, we show in Fig. 14 the averaged experimental streamlines over a period for both rolling-grain ripples and vortex ripples. Both types of ripples feature two contrarotating cells.

V. CONCLUSIONS

We were able to see for the first time the flow pattern, especially a transient eddy or vortex above real rolling-grain ripples in water. The morphological evolution of this structure is well predicted by the theory on the flow over a no-slip rigid wavy wall that only takes into account the $O(\epsilon)$-order effect of the ripple height. The existence of eddies or vortices over two kinds of ripples is similar to the steady structure over a backward-facing step or a sudden expansion, where a viscous weak eddy characterized by Moffatt[25] appears for very low Reynolds number and typical separation vortices at higher Reynolds number. The appearance of transient vorti-

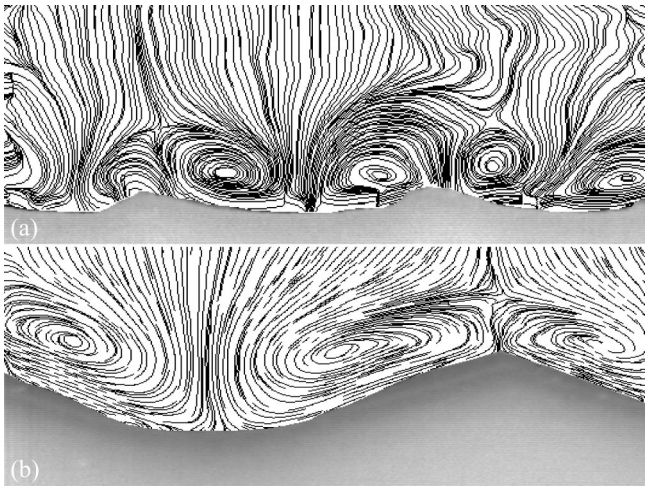

FIG. 14. Averaged streamlines over a period (250 pictures/s): (a) rolling-grain ripples ($t^*f=1620$); (b) vortex ripples ($t^*f=5700$), for $A=15$ mm, $f=1$ Hz, and $d=0.11$ mm.

ces above a ripple bed was generally assumed to be the dynamical signature of vortex ripple patterns, whereas our very careful experiments show that rolling-grain ripples also feature a transient coherent hydrodynamical structure. The existence of the coherent structure that was observed both experimentally and numerically raises an essential question about the difference in the sand transport between the rolling-grain ripples and the vortex ripples as both feature such a coherent structure during the flow reversal. Our calculations show that linear analysis is robust and still predicts the eddy's characteristics despite some discrepancies in the bottom layer for $\epsilon \sim 1$. Future works should concentrate on the role of these two different flow configurations on the erosion mechanism in each kind of ripple (rolling-grain and vortex ripples).

ACKNOWLEDGMENTS

We are grateful to Denis Vallet, Olivier Brouard, and Christian Baradel for technical help. This work was supported by the A.C.I. ''Jeunes chercheurs'' Grant No. 2314. We thank S. Davis and S. Cuevas for fruitful discussions on steady streamings.

[1] R. A. Bagnold, ''Motion of waves in shallow water. Interaction between waves and sand bottoms. With an additional note by Sir G. I. Taylor,'' Proc. R. Soc. London, Ser. A **187**, 1 (1946).
[2] A. Stegner and J.-E. Wesfreid, ''Dynamical evolution of sand ripples under water,'' Phys. Rev. E **60**, 3487 (1999).
[3] J. F. A. Sleath, *Sea Bed Mechanics* (Wiley, New York, 1984).
[4] N. Riley, ''Steady streaming,'' Annu. Rev. Fluid Mech. **33**, 43 (2001).
[5] L. Petit and P. Gondret, ''Redressement d'un écoulement alternatif,'' J. Phys. II **2**, 2115 (1992).
[6] S. Cuevas and G. Huelsz, ''Oscillatory boundary-layer flows,'' Recent Res. Dev. Fluid Dyn. **2**, 35 (1999).
[7] W. H. Lyne, ''Unsteady viscous flow over a wavy wall,'' J. Fluid Mech. **50**, 33 (1971).
[8] J. F. A. Sleath, ''On rolling-grain ripples,'' J. Hydraul. Res. **14**, 69 (1976).
[9] A. Kaneko and H. Honji, ''Double structures of steady streaming in the oscillatory viscous flow over a wavy wall,'' J. Fluid Mech. **93**, 727 (1979).
[10] S. Cuevas, F. Z. Sierra, and A. A. Avramenko, ''Magnetic damping of steady streaming vortices in an oscillatory viscous flow over a wavy wall,'' Magnetohydrodynamics (N.Y.) **38**, 345 (2002).
[11] G. Vittori, ''Non-linear viscous oscillatory flow over a small amplitude wavy wall,'' J. Hydraul. Res. **27**, 267 (1989).
[12] P. Blondeaux, ''Sand ripples under sea-waves. Part 1. Ripple formation,'' J. Fluid Mech. **218**, 1 (1990).
[13] G. Vittori and P. Blondeaux, ''Sand ripples under sea-waves. Part 2. Finite-amplitude development,'' J. Fluid Mech. **218**, 19 (1990).
[14] N. Matsunaga, A. Kaneko, and H. Honji, ''A numerical study of steady streamings in the oscillatory flow over a wavy wall,'' J. Hydraul. Res. **19**, 29 (1981).
[15] T. Hara and C. C. Mei, ''Oscillating flow over periodic ripples,'' J. Fluid Mech. **211**, 183 (1990).
[16] G. Rousseaux, A. Stegner, and J.-E. Wesfreid, ''Wavelength selection of rolling grains ripples in the laboratory'' (preprint, 2003).
[17] K. Andersen, ''The dynamics of ripples beneath surface waves,'' Ph.D. thesis, Niels Bohr Institute, 1999 (http://www.nbi.dk/~kenand).
[18] C. Faraci and E. Foti, ''Evolution of small scale regular patterns generated by waves propagating over a sandy bottom,'' Phys. Fluids **13**, 1624 (2001).
[19] M. A. Scherer, F. Melo, and M. Marder, ''Sand ripples in an oscillating sand-water cell,'' Phys. Fluids **11**, 58 (1999).
[20] H. Honji, A. Kaneko, and N. Matsunaga, ''Flow above oscillatory ripples,'' Sedimentology **27**, 225 (1980).
[21] E. Guyon, L. Petit, J. P. Hulin, and C. Mitescu, *Physical Hydrodynamics* (Oxford University Press, Oxford, 2001).
[22] T. Hara, C. C. Mei, and K. T. Shum, ''Oscillatory flow over periodic ripples of finite slope,'' Phys. Fluids A **4**, 1373 (1992).
[23] P. L. F. Liu, M. H. Davis, and S. Downing, ''Wave-induced boundary layer flows above and in a permeable bed,'' J. Fluid Mech. **325**, 195 (1996).
[24] S.-C. Hsiao and P. L. F. Liu, ''The porous effect on the bottom instability under partially standing waves,'' Chin. J. Mech. Ser. A **18**, 53 (2002).
[25] H. K. Moffatt, ''Viscous and resistive eddies near a sharp corner,'' J. Fluid Mech. **18**, 1 (1964).
[26] N. Alleborn, K. Nandakumar, H. Raszillier, and F. Durst, ''Further contributions on the two-dimensional flow in a sudden expansion,'' J. Fluid Mech. **330**, 169 (1997).